Formation, Characterization, and Reactivity of Bis(μ-oxo)dinickel(III) Complexes Supported by A Series of Bis[2-(2-pyridyl)ethyl]amine Ligands

Shinobu Itoh,*,† Hideki Bandoh,‡ Motonobu Nakagawa,‡ Shigenori Nagatomo,¶ Teizo Kitagawa,*,¶ Kenneth D. Karlin,§ and Shunichi Fukuzumi*,‡

Contribution from the Department of Chemistry, Graduate School of Science, Osaka City University, 3-3-138, Sugimoto, Sumiyoshi-ku, Osaka, 558-8585, Japan, Department of Material and Life Science, Graduate School of Engineering, Osaka University, CREST, Japan Science and Technology Corporation, 2-1 Yamada-oka, Suita, Osaka 565-0871, Japan, Institute for Molecular Science, Myodaiji, Okazaki 444-8585, Japan, and Department of Chemistry, Johns Hopkins University, Baltimore, Maryland 21218

Received February 15, 2001. Revised Manuscript Received August 18, 2001

Abstract: Bis(μ-oxo)dinickel(III) complexes supported by a series of bis[2-(2-pyridyl)ethyl]amine ligands have been successfully generated by treating the corresponding bis(μ-hydroxo)dinickel(II) complexes or bis(μ-methoxo)dinickel(II) complex with an equimolar amount of H_2O_2 in acetone at low temperature. The bis(μ-oxo)dinickel(III) complexes exhibit a characteristic UV−vis absorption band at ∼410 nm and a resonance Raman band at 600−610 cm^{-1} that shifted to 570−580 cm^{-1} upon ^{18}O-substitution. Kinetic studies and isotope labeling experiments using $^{18}O_2$ imply the existence of intermediate(s) such as peroxo dinickel(II) in the course of formation of the bis(μ-oxo)dinickel(III) complex. The bis(μ-oxo)dinickel(III) complexes supported by the mononucleating ligands (**L1^X** = para-substituted *N*,*N*-bis[2-(2-pyridyl)ethyl]-2-phenylethylamine; X = OMe, Me, H, Cl) gradually decompose, leading to benzylic hydroxylation of the ligand side arm (phenethyl group). The kinetics of the ligand hydroxylation process including kinetic deuterium isotope effects (KIE), *p*-substituent effects (Hammett plot), and activation parameters ($\Delta H_H^{\ddagger}$ and $\Delta S_H^{\ddagger}$) indicate that the bis(μ-oxo)dinickel(III) complex exhibits an ability of hydrogen atom abstraction from the substrate moiety as in the case of the bis(μ-oxo)dicopper(III) complex. Such a reactivity of bis(μ-oxo)dinickel(III) complexes has also been suggested by the observed reactivity toward external substrates such as phenol derivatives and 1,4-cyclohexadiene. The thermal stability of the bis(μ-oxo)dinickel(III) complex is significantly enhanced when the dinucleating ligand with a longer alkyl strap is adopted instead of the mononucleating ligand. In the *m*-xylyl ligand system, no aromatic ligand hydroxylation occurred, showing a sharp contrast with the reactivity of the (μ-η^2:η^2-peroxo)-dicopper(II) complex with the same ligand which induces aromatic ligand hydroxylation via an electrophilic aromatic substitution mechanism. Differences in the structure and reactivity of the active oxygen complexes between the nickel and the copper systems are discussed on the basis of the detailed comparison of these two systems with the same ligand.

Introduction

Dioxygen activation by transition-metal complexes is one of the most important and attractive research objectives not only in bioinorganic chemistry but also in numerous and diverse array of catalytic oxidation reactions.[1−3] Great efforts have so far been focused on the mechanism of iron−porphyrin systems, particularly cytochrome P-450, where an Fe(IV)═O porphyrin (Por) π-cation radical has been suggested to form via heterolytic O−O bond cleavage of a (Por)Fe(III)−OOH intermediate.[1−4] More recently, active oxygen species of non-heme transition-metal complexes have attracted much interest in relation to active oxygen intermediates of a growing number of non-heme monooxygenases.[1−3,5−13] Among a series of active oxygen species of mono-, di-, and oligonuclear transition-metal complexes, high-valent bimetallic bis(μ-oxo) complexes, M(μ-O)$_2$M,

† Osaka City University.
‡ Osaka University.
¶ Institute for Molecular Science.
§ Johns Hopkins University.

(1) (a) Valentine, J. S., Foote, C. S., Greenberg, A., Liebman, J. F., Eds. *Active Oxygen in Biochemistry*; Chapman and Hall: London, 1995. (b) Foote, C. S., Valentine, J. S., Greenberg, A., Liebman, J. F., Eds. *Active Oxygen in Chemistry*; Chapman and Hall: London, 1995.
(2) Funabiki, T., Ed. *Oxygenases and Model Systems*; Kluwer Academic Publishers: Dordrecht, 1997.
(3) (a) Meunier, B., Ed. *Biomimetic Oxidations Catalyzed by Transition Metal Complexes*; Imperial College Press: London, 1999. (b) Meunier, B., Ed. *Metal−Oxo and Metal−Peroxo Species in Catalytic Oxidations*; Springer: Berlin, 2000.
(4) Ortiz de Montellano, P. R., Ed. *Cytochrome P-450. Structure, Mechanism, and Biochemistry*; Plenum Press: New York, 1986.
(5) Karlin, K. D., Tyeklár, Z., Eds. *Bioinorganic Chemistry of Copper*; Chapman and Hall: New York, 1993.
(6) Kitajima, N.; Moro-oka, Y. *Chem. Rev.* **1994**, *94*, 737−757.
(7) Feig, A. L.; Lippard, S. J. *Chem. Rev.* **1994**, *94*, 759−805.
(8) Pecoraro, V. L.; Baldwin, M. J.; Gelasco, A. *Chem. Rev.* **1994**, *94*, 807−826.
(9) Solomon, E. I.; Tuczek, F.; Root, D. E.; Brown, C. A. *Chem. Rev.* **1994**, *94*, 827−856.
(10) Shilvo, A. E.; Shul'pin, G. B. *Chem. Rev.* **1997**, *97*, 2879−2932.
(11) Valentine, A. M.; Lippard, S. J. *J. Chem. Soc., Dalton Trans.* **1997**, 3925−3931.
(12) Que, L., Jr. *J. Chem. Soc., Dalton Trans.* **1997**, 3933−3940.
(13) Tolman, W. B. *Acc. Chem. Res.* **1997**, *30*, 227−237.

10.1021/ja0104094 CCC: $20.00
Published on Web 10/17/2001

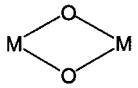

$[M(\mu\text{-}O)_2M]$

have recently attracted particular attention as possible reaction intermediates of the dioxygen-activating enzymes having a dinuclear iron or copper active center.[11−15] Such a bimetallic bis(μ-oxo) complex (M = Mn) has also been suggested to be involved in the dioxygen evolution in photosystem II.[16,17]

The structures of high-valent bimetallic bis(μ-oxo) complexes, $M(\mu\text{-}O)_2M$, have so far been well characterized by X-ray crystallographic analyses on those of M = Fe, Cu, Mn, Co, and Ni.[18−23] In particular, the structural characterizations of $Fe^{III}(\mu\text{-}O)_2Fe^{IV}$ by Que et al.[18] and $Cu^{III}(\mu\text{-}O)_2Cu^{III}$ by Tolman et al., Stack et al., and others[19] have provided profound insight into the dioxygen activation mechanism by the non-heme monooxygenases. However, mechanistic details of the formation process of such active-oxygen complexes have yet to be elucidated. The reactivity of $M(\mu\text{-}O)_2M$ complexes of M = Fe, Cu, and Mn has also been explored in relation to aliphatic or aromatic C−H bond activation involved in the reactions of methane monooxygenases (MMO) and related enzymes.[24−28]

To fully understand the C−H bond activation mechanism by $M(\mu\text{-}O)_2M$ complexes, it is highly desired to compare the reactivity of the bimetallic bis(μ-oxo) complexes using different transition-metal ions and ligands. In this context, we have recently reported that a $Ni^{III}(\mu\text{-}O)_2Ni^{III}$ complex supported by para-substituted *N*,*N*-bis[2-(2-pyridyl)ethyl]-2-phenylethylamine (**L1^X**, X = OMe, Me, H, Cl; see Chart 1) shows a reactivity similar to that of the bis(μ-oxo)dicopper(III) complexes, leading to aliphatic hydroxylation of the ligand side arm at its benzylic position.[29] The $Ni^{III}(\mu\text{-}O)_2Ni^{III}$ complex was derived from the corresponding bis(μ-hydroxo)dinickel(II) complex, $[\mathbf{L1^X}Ni^{II}(\mu\text{-}OH)_2Ni^{II}\mathbf{L1^X}]^{2+}$, and hydrogen peroxide at a low temperature (eq 1).[29] This is in sharp contrast to the case of the copper(II) complex with the same ligand, where a $(\mu\text{-}\eta^2\text{:}\eta^2\text{-peroxo})$-dicopper(II) complex rather than a bis(μ-oxo)dicopper(III) complex was predominantly formed.[30] Thus, it is obvious that the metal ion plays a critical role in enhancing the O−O bond homolysis of the peroxo species.

Chart 1

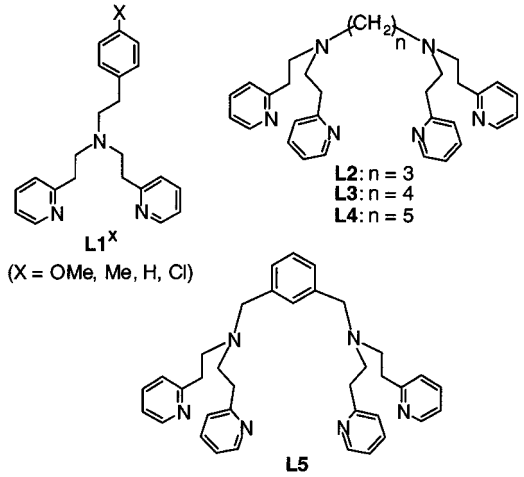

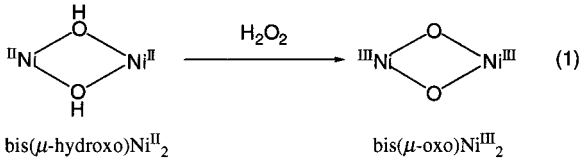

We report herein the first systematic studies on spectroscopic features and the formation mechanism as well as the reactivity of the $Ni^{III}(\mu\text{-}O)_2Ni^{III}$ complexes, to shed light further on the dioxygen activation mechanism by non-heme transition-metal complexes. In addition to **L1^X** ligands, a series of alkyl-strapped dinucleating ligands **L2**−**L5** (Chart 1) containing the bis[2-(2-pyridyl)ethyl]amine moiety[31−33] has also been employed to examine the ligand effects on the structure and reactivity of the $Ni^{III}(\mu\text{-}O)_2Ni^{III}$ complexes. The oxidation of external substrates by the $Ni^{III}(\mu\text{-}O)_2Ni^{III}$ complexes is also reported under the experimental conditions such that the aliphatic ligand hydroxylation is negligible as compared to the oxidation of external substrates. This study provides an excellent opportunity to examine the effects of metal ions on the structure and reactivity of the active oxygen species.

Results and Discussion

Characterization of Bis(μ-hydroxo)dinickel(II) and Bis(μ-methoxo)dinickel(II) Complexes. The mono- and dinucle-

(14) Shu, L.; Nesheim, J. C.; Kauffmann, K.; Münck, E.; Lipscomb, J. D.; Que, L., Jr. *Science* **1997**, *275*, 515−518.
(15) Elliott, S. J.; Zhu, M.; Tso, L.; Nguyen, H.-H. T.; Yip, J. H.-K.; Chan, S. I. *J. Am. Chem. Soc*. **1997**, *119*, 9949−9955.
(16) Tommos, C.; Babcock, G. T. *Acc. Chem. Res*. **1998**, *31*, 18−25.
(17) Ruttinger, W.; Dismukes, G. C. *Chem. Rev*. **1997**, *97*, 1−24.
(18) Hsu, H.-F.; Dong, Y.; Shu, L.; Young, V. G., Jr.; Que, L., Jr. *J. Am. Chem. Soc*. **1999**, *121*, 5230−5237.
(19) (a) Halfen, J. A.; Mahapatra, S.; Wilkinson, E. C.; Kaderli, S.; Young, V. G., Jr.; Que, L., Jr.; Tolman, W. B. *Science* **1996**, *271*, 1397−1400. (b) Mahapatra, S.; Halfen, J. A.; Wilkinson, E. C.; Pan, G.; Wang, X.; Young, V. G., Jr.; Cramer, C. J.; Que, L., Jr.; Tolman, W. B. *J. Am. Chem. Soc*. **1996**, *118*, 11555−11574. (c) Mahadevan, V.; Hou, Z.; Cole, A. P.; Root, D. E.; Lal, T. K.; Solomon, E. I.; Stack, T. D. P. *J. Am. Chem. Soc*. **1997**, *119*, 11996−11997. (d) Hayashi, H.; Fujinami, S.; Nagatomo, S.; Ogo, S.; Suzuki, M.; Uehara, A.; Watanabe, Y.; Kitagawa, T. *J. Am. Chem. Soc*. **2000**, *122*, 2124−2125. (e) Straub, B. F.; Rominger, F.; Hofmann, P. *Chem. Commun*. **2000**, 1611−1612.
(20) (a) Que, L., Jr.; True, A. E. *Prog. Inorg. Chem*. **1990**, *38*, 97−200. (b) Lal, T. K.; Mukherjee, R. *Inorg. Chem*. **1998**, *37*, 2373−2382 and references therein.
(21) Limburg, J.; Vrettos, J. S.; Liable-Sands, L. M.; Rheingold, A. L.; Crabtree, R. H.; Brudvig, G. W. *Science* **1999**, *283*, 1524−1527.
(22) Hikichi, S.; Yoshizawa, M.; Sasakura, Y.; Akita, M.; Moro-ka, Y. *J. Am. Chem. Soc*. **1998**, *120*, 10567−10568.
(23) Shiren, K.; Ogo, S.; Fujinami, S.; Hayashi, H.; Suzuki, M.; Uehara, A.; Watanabe, Y.; Moro-oka, Y. *J. Am. Chem. Soc*. **2000**, *122*, 254−262.
(24) Kim, C.; Dong, Y.; Que, L., Jr. *J. Am. Chem. Soc*. **1997**, *119*, 3635−3636.
(25) Mahapatra, S.; Halfen, J. A.; Tolman, W. B. *J. Am. Chem. Soc*. **1996**, *118*, 11575−11586.
(26) Itoh, S.; Taki, M.; Nakao, H.; Holland, P. L.; Tolman, W. B.; Que, L., Jr.; Fukuzumi, S. *Angew. Chem*. **2000**, *112*, 409−411; *Angew. Chem., Int. Ed*. **2000**, *39*, 398−400.
(27) (a) Mahadevan, V.; DuBois, J. L.; Hedman, B.; Hodgson, K. O.; Stack, T. D. P. *J. Am. Chem. Soc*. **1999**, *121*, 5583−5584. (b) Mahadevan, V.; Henson, M. J.; Solomon, E. I.; Stack, T. D. P. *J. Am. Chem. Soc*. **2000**, *122*, 10249−10250.
(28) (a) Wang, K.; Mayer, J. M. *J. Am. Chem. Soc*. **1997**, *119*, 1470−1471. (b) Lockwood, M. A.; Wang, K.; Mayer, J. M. *J. Am. Chem. Soc*. **1999**, *121*, 11894−11895.
(29) Itoh, S.; Bandoh, H.; Nagatomo, S.; Kitagawa, T.; Fukuzumi, S. *J. Am. Chem. Soc*. **1999**, *121*, 8945−8946.
(30) (a) Itoh, S.; Kondo, T.; Komatsu, M.; Ohshiro, Y.; Li, C.; Kanehisa, N.; Kai, Y.; Fukuzumi, S. *J. Am. Chem. Soc*. **1995**, *117*, 4714−4715. (b) Itoh, S.; Nakao, H.; Berreau, L. M.; Kondo, T.; Komatsu, M.; Fukuzumi, S. *J. Am. Chem. Soc*. **1998**, *120*, 2890−2899.
(31) Karlin, K. D.; Haka, M. S.; Cruse, R. W.; Meyer, G. J.; Farooq, A.; Gultneh, Y.; Hayes, J. C.; Zubieta, J. *J. Am. Chem. Soc*. **1988**, *110*, 1196−1207.
(32) Karlin, K. D.; Tyeklár, Z.; Farooq, A.; Haka, M. S.; Ghosh, P.; Cruse, R. W.; Gultneh, Y.; Hayes, J. C.; Toscano, P. J.; Zubieta, J. *Inorg. Chem*. **1992**, *31*, 1436−1451.
(33) Karlin, K. D.; Hayes, J. C.; Gultneh, Y.; Cruse, R. W.; McKown, J. W.; Hutchinson, J. P.; Zubieta, J. *J. Am. Chem. Soc*. **1984**, *106*, 2121−2128.

Table 1. Summary of X-ray Crystallographic Data

	$[(\mathbf{L1^H}Ni^{II})_2(\mu\text{-}OH)_2](ClO_4)_2$	$[(\mathbf{L4})(Ni^{II})_2(\mu\text{-}OMe)_2](ClO_4)_2\cdot MeCN\cdot MeOH$
empirical formula	$C_{44}H_{52}N_6O_{10}Ni_2Cl_2$	$C_{38}H_{55}N_7O_{11}Ni_2Cl_2$
formula weight	1013.24	974.20
crystal system	monoclinic	orthorhombic
space group	$P2_1/n$ (No. 14)	$P2_12_12_1$ (No. 19)
a, Å	10.2036(8)	12.1118(2)
b, Å	16.656(1)	33.1982(5)
c, Å	13.363(1)	11.0644(1)
β, deg	105.302(3)	
V, Å^3	2190.6(3)	4448.88(9)
Z	2	4
F(000)	1056.00	2040.00
D_{calc}, g/cm^3	1.536	1.454
T, °C	−150	−150
crystal size, mm	0.30 × 0.30 × 0.20	0.30 × 0.30 × 0.20
μ (MoKα), cm^{-1}	10.48	10.31
diffractometer	Rigaku RAXIS−RAPID	Rigaku RAXIS−RAPID
radiation	MoKα (0.71069 Å)	MoKα (0.71069 Å)
$2\theta_{max}$, deg	55.0	55.0
no. of reflns measd	5206	5623
no. of reflns obsd [$I > 3\sigma(I)$]	3274	3313
no. of variables	450	501
R^a	0.041	0.045
wR^b	0.058	0.063

[a] $R = \sum||F_o| - |F_c||/\sum|F_o|$. [b] $wR = \{\sum w(|F_o| - |F_c|)^2/\sum wF_o^2\}^{1/2}$.

ating ligands **L1^X**−**L5** were prepared according to the reported procedures.[30−33] Bis(μ-hydroxo)dinickel(II) complexes have been prepared as the starting materials by treating the ligands and $Ni(ClO_4)_2\cdot 6H_2O$ in the presence of triethylamine in ethanol. The complexes exhibit characteristically sharp absorption bands due to the μ-OH group around 3600 cm^{-1} in the FT-IR spectra (see Experimental Section).

Single crystals of $[(\mathbf{L1^H}Ni^{II})_2(\mu\text{-}OH)_2](ClO_4)_2$ were obtained by vapor diffusion of ether into an MeCN solution of the complex. Single crystals of a bis(μ-methoxo)dinickel(II) complex supported by **L4**, $[(\mathbf{L4})(Ni^{II})_2(\mu\text{-}OMe)_2](ClO_4)_2\cdot MeCN\cdot MeOH$, were obtained when the bis(μ-hydroxo)dinickel(II) complex of **L4** was recrystallized from a 1:1 mixture of MeOH and MeCN. The crystallographic data are summarized in Table 1 together with the ORTEP drawings of the cationic parts of the complexes as shown in Figures 1 and 2. Selected bond distances and angles are also presented in Table 2.[34] The bis(μ-hydroxo)dinickel(II) complex supported by **L1^H** has an imposed center of symmetry and consists of five-coordinated nickel centers with a square pyramidal geometry, where each basal plane consists of two pyridine nitrogen atoms, N(1), N(2) and N(1)*, N(2)*, and two bridging oxygen atoms, O(1) and O(1)*, whereas the axial position is occupied by the tertiary amine nitrogen, N(3) and N(3)* ($\tau = 0.07$).[35] The configuration of the axial Ni−N bond of each metal center is anti, and the two phenethyl groups cover the bis(μ-hydroxo)dinickel core from the top and the bottom, as shown in Figure 1. The average bond lengths of Ni−O (1.991 Å) and Ni−N (2.067 Å) are a little shorter than those of the six-coordinated bis(μ-hydroxo)-dinickel(II) complexes supported by the tetradentate tris(2-pyridylmethyl)amine (TPA) derivatives.[23,36]

The bis(μ-methoxo)dinickel(II) complex supported by the dinucleating ligand **L4**, $[(\mathbf{L4})(Ni^{II})_2(\mu\text{-}OMe)_2](ClO_4)_2\cdot MeCN\cdot MeOH$, has an approximate *C*2 symmetry, and both nickel centers also have square pyramidal structures, where each basal plane consists of two pyridine nitrogen atoms, N(1), N(2) and N(4), N(5), and two bridging oxygen atoms of the methoxo groups, O(1) and O(2), whereas the axial positions are occupied by the tertiary amine nitrogens N(3) and N(6). The square pyramidal structure in this case is, however, significantly distorted ($\tau = 0.25$ and 0.36) as compared to that of the **L1^H** complex, and the bis(μ-methoxo)dinickel core is bent about 16° along the O(1)−O(2) axis. The structural distortion is due to the alkyl strap which induces the syn configuration of the two axial Ni−N bonds as shown in Figure 2. The average bond lengths of Ni−O (1.987 Å) and Ni−N (2.066 Å) in $[(\mathbf{L4})(Ni^{II})_2(\mu\text{-}OMe)_2]^{2+}$ are in the same range as those of $[(\mathbf{L1^H}Ni^{II})_2(\mu\text{-}OH)_2]^{2+}$.

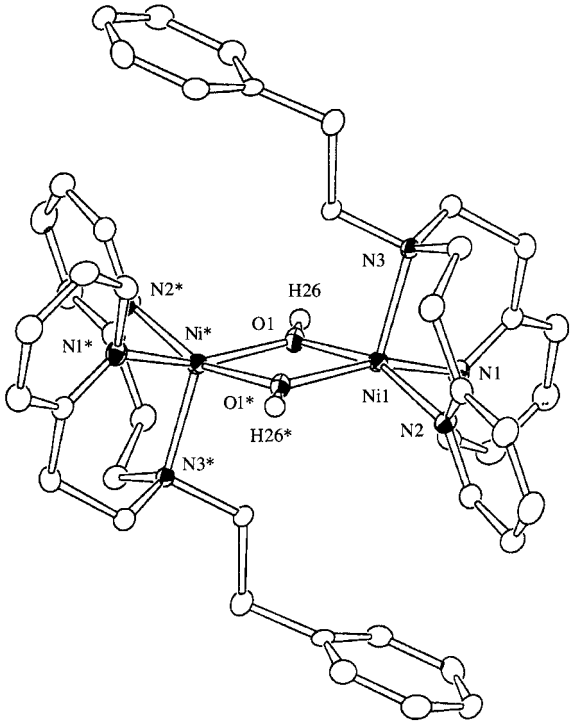

Figure 1. ORTEP drawing of the cationic part of $[(\mathbf{L1^H}Ni^{II})_2(\mu\text{-}OH)_2](ClO_4)_2$. The counteranions and hydrogen atoms are omitted for clarity.

(34) Atomic coordinates, thermal parameters, and intramolecular bond distances and angles have been deposited in the Supporting Information (CIF file format).

(35) Addison, A. W.; Rao, T. N. *J. Chem. Soc., Dalton Trans.* **1984**, 1349−1356.

(36) Ito, M.; Sakai, K.; Tsubomura, T.; Takita, Y. *Bull. Chem. Soc. Jpn.* **1999**, *72*, 239−247.

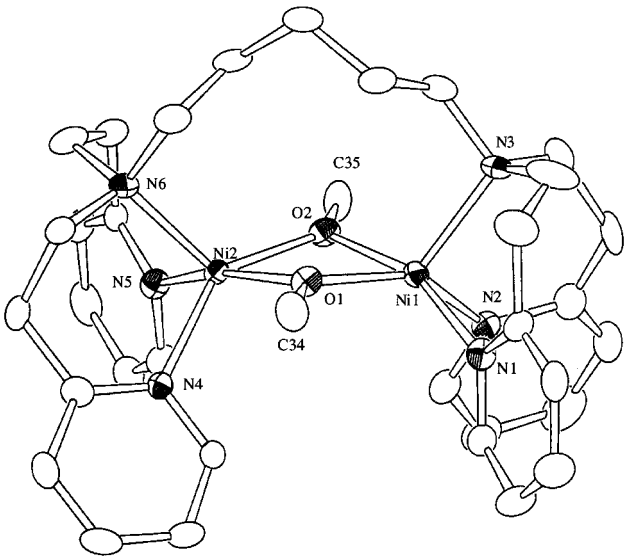

Figure 2. ORTEP drawing of the cationic part of $[(\mathbf{L4})(Ni^{II})_2(\mu\text{-}OMe)_2](ClO_4)_2\cdot MeCN\cdot MeOH$. The solvents, counteranions, and hydrogen atoms are omitted for clarity.

Table 2. Selected Bond Lengths (Å) and Angles (deg)[a]

	$[(\mathbf{L1^H}Ni^{II})_2(\mu\text{-}OH)_2](ClO_4)_2$		
Ni(1)−O(1)	1.979(2)	Ni(1)−O(1)*	2.003(2)
Ni(1)−N(1)	2.052(3)	Ni(1)−N(2)	2.071(3)
Ni(1)−N(3)	2.079(3)	Ni(1)−Ni(1)*	3.11
O(1)−O(1)*	2.49		
O(1)−Ni(1)-O(1)*	77.4(1)	O(1)−Ni(1)−N(1)	155.94(9)
O(1)−Ni(1)-N(2)	91.7(1)	O(1)−Ni(1)−N(3)	105.30(10)
O(1)*−Ni(1)−N(1)	89.2(1)	O(1)−Ni(1)−N(2)	160.0(10)
O(1)*−Ni(1)−N(3)	102.15(10)	N(1)−Ni(1)−N(2)	94.6(1)
N(1)−Ni(1)−N(3)	96.9(1)	N(2)−Ni(1)−N(3)	96.8(1)
Ni(1)−O(1)−Ni(1)*	102.6(1)		
	$[(\mathbf{L4})(Ni^{II})_2(\mu\text{-}OMe)_2](ClO_4)_2\cdot MeCN\cdot MeOH$		
Ni(1)−O(1)	1.972(6)	Ni(2)−O(1)	2.014(6)
Ni(1)−O(2)	1.997(6)	Ni(2)−O(2)	1.957(6)
Ni(1)−N(1)	2.051(7)	Ni(2)−N(4)	2.069(7)
Ni(1)−N(2)	2.071(7)	Ni(2)−N(5)	2.051(7)
Ni(1)−N(3)	2.080(7)	Ni(2)−N(6)	2.076(7)
Ni(1)−Ni(2)	3.09	O(1)−O(2)	2.43
O(1)−Ni(1)−O(2)	75.6(2)	O(1)−Ni(2)−O(2)	75.5(2)
O(1)−Ni(1)−N(1)	92.7(3)	O(1)−Ni(2)−N(4)	88.5(2)
O(1)−Ni(1)−N(2)	144.9(3)	O(1)−Ni(2)−N(5)	161.4(2)
O(1)−Ni(1)−N(3)	117.2(3)	O(1)-Ni(2)-N(6)	104.8(3)
O(2)−Ni(1)−N(1)	160.0(3)	O(2)-Ni(2)-N(4)	139.7(2)
O(2)−Ni(1)−N(2)	89.8(3)	O(2)−Ni(2)−N(5)	92.1(3)
O(2)−Ni(1)−N(3)	105.2(3)	O(2)−Ni(2)−N(6)	121.6(3)
N(1)−Ni(1)−N(2)	90.9(3)	N(4)−Ni(2)−N(5)	92.3(3)
N(1)−Ni(1)−N(3)	94.5(3)	N(4)−Ni(2)−N(6)	98.0(3)
N(2)−Ni(1)−N(3)	97.3(3)	N(5)−Ni(2)−N(6)	93.6(3)
N(1)−O(1)−Ni(2)	101.7(2)	Ni(1)−O(2)−Ni(2)	102.9(2)

[a] Estimated standard deviations are given in parentheses.

The bis(μ-hydroxo)dinickel(II) complex, $[(\mathbf{L1^H}Ni^{II})_2(\mu\text{-}OH)_2]^{2+}$, exhibits a reversible redox couple at 0.66 V vs Fc/Fc^+ in acetone containing 0.01 M $n\text{-}Bu_4N(ClO_4)$, as shown in Figure 3. The redox couple corresponds to the one-electron oxidation of the Ni(II)Ni(II) state to the Ni(II)Ni(III) state. The bis(μ-hydroxo)dinickel(II) complexes supported by the dinucleating ligands **L2**−**L5** have a redox couple in a slightly higher potential region ($E_{1/2} = 0.71-0.78$ V vs Fc/Fc^+, Table 3). The reversibility of these couples was, however, worse as compared to that of the redox couple of $[(\mathbf{L1^H}Ni^{II})_2(\mu\text{-}OH)_2]^{2+}$, as indicated by the larger ΔE_p values in Table 3. This may be due to the lower flexibility of the dinickel core in the dinucleating ligand system (**L2**−**L5**) as compared to the mononucleating analogue

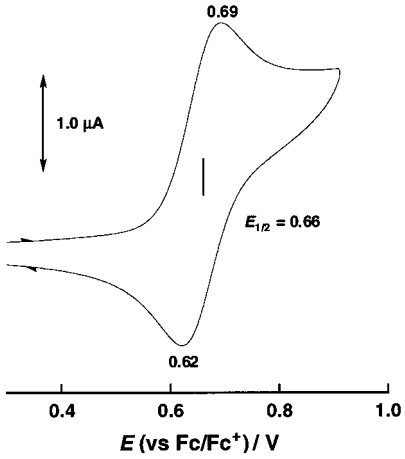

Figure 3. Cyclic voltammogram of $[(\mathbf{L1^H}Ni^{II})_2(\mu\text{-}OH)_2](ClO_4)_2$ (5.0×10^{-4} M) in deaerated acetone containing 0.01 M $n\text{-}Bu_4NClO_4$ at 25 °C; working electrode, Pt; counter electrode, Pt; reference electrode, Fc/Fc^+; sweep rate, 100 mV s^{-1}.

Table 3. Cyclic Voltammetric Data for the Oxidation of Bis(μ-hydroxo)dinickel(II) Complexes in Acetone (E vs Fc/Fc^+/V)

complex	E^a_p	E^c_p	ΔE_p	$E_{1/2}$
$[(\mathbf{L1^H}Ni^{II})_2(\mu\text{-}OH)_2]^{2+}$	0.69	0.62	0.07	0.66
$[(\mathbf{L2})(Ni^{II})_2(\mu\text{-}OH)_2]^{2+}$	0.77	0.65	0.12	0.71
$[(\mathbf{L3})(Ni^{II})_2(\mu\text{-}OH)_2]^{2+}$	0.80	0.68	0.18	0.74
$[(\mathbf{L4})(Ni^{II})^2(\mu\text{-}OH)_2]^{2+}$	0.86	0.69	0.17	0.78
$[(\mathbf{L5})(Ni^{II})_2(\mu\text{-}OH)_2]^{2+}$	0.81	0.64	0.17	0.73
$[(\mathbf{L4})(Ni^{II})_2(\mu\text{-}OH)_2]^{2+}$	1.07	0.78	0.29	0.93

($\mathbf{L1^H}$). This indicates that the alkyl strap in **L2**−**L5** holds the bis(μ-hydroxo)dinickel(II) core more tightly, thus preventing the geometrical change induced by the electrochemical redox reaction. Since the average values of the Ni−O and Ni−N bond lengths between $[(\mathbf{L1^H}Ni^{II})_2(\mu\text{-}OH)_2]^{2+}$ and $[(\mathbf{L4})(Ni^{II})_2(\mu\text{-}OMe)_2]^{2+}$ are nearly the same within experimental error (Table 2), the increment of the oxidation potential $E_{1/2}$ in the binucleating ligand system (**L2**−**L5**) may be attributable to the structural distortion induced by the alkyl strap. The lower $E_{1/2}$ value of the bis(μ-hydroxo)dinickel(II) than that of the bis(μ-methoxo)dinickel(II) with the same ligand **L4** may be attributed to the existence of a dissociable proton in the μ-hydroxo bridging ligand. Namely, partial dissociation of the μ-OH proton will enhance the donor ability of the bridging oxygen atom to stabilize the Ni(III) state to some extent.

Reaction with Hydrogen Peroxide. Addition of just 1 equiv of H_2O_2 into an acetone solution of the bis(μ-hydroxo)dinickel(II) complex at a low temperature resulted in a color change from light blue to dark brown. The spectral change in the reaction of $[(\mathbf{L1^H}Ni^{II})_2(\mu\text{-}OH)_2]^{2+}$ and H_2O_2 is shown in Figure 4 as a typical example, where a characteristic absorption band at 408 nm ($\epsilon = 6000$ M^{-1} cm^{-1}) due to an intermediate appears in the course of the reaction. Similar spectral changes have been observed in the reactions of H_2O_2 with other bis(μ-hydroxo)dinickel(II) complexes of ligands **L2**−**L5**, and their λ_{max} values and molar absorption coefficients (ϵ) are summarized in Table 4. The characteristic absorption bands around 410 nm and their ϵ values are fairly close to those of the structurally characterized bis(μ-oxo)dinickel(III) complexes (i.e., those of Hikichi et al., $\lambda_{max} = 410$ nm, $\epsilon = 4200$ M^{-1} cm^{-1}, and those of Suzuki and co-workers, $\lambda_{max} = 394$ nm, $\epsilon = 4000$ M^{-1} cm^{-1}),[22,23] although the ϵ value of $[(\mathbf{L5})(Ni^{III})_2(\mu\text{-}O)_2]^{2+}$ is considerably smaller (1200 M^{-1} cm^{-1}).[37] Such a characteristic absorption band around 410 nm can be assigned to oxo-to-metal charge transfer (LMCT) as in the case of the bis(μ-oxo)dicopper(III) complex,

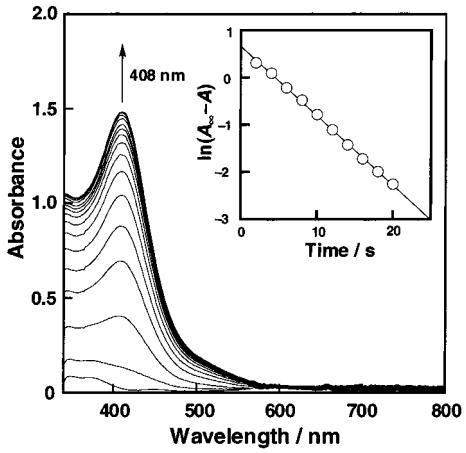

Figure 4. Spectral change observed upon addition of 1 equiv of H_2O_2 into an acetone solution of $[(\mathbf{L1^H}Ni^{II})_2(\mu\text{-}OH)_2](ClO_4)_2$ (2.5×10^{-4} M) at −90 °C in a 1 cm path length UV cell (2 s interval). Inset: First-order plot based on the absorption change at 408 nm.

Table 4. UV−Vis and Resonance Raman Data of the Intermediates[a]

	UV−vis		Raman		
complex	λ_{max}, nm	ϵ, M^{-1} cm^{-1}	$\nu(^{16}O)$	$\nu(^{18}O)$	$\Delta\nu$
$[(\mathbf{L1^H}Ni^{III})_2(\mu\text{-}O)_2]^{2+}$	408	6000	612	580	32
$[(\mathbf{L2})(Ni^{III})_2(\mu\text{-}O)_2]^{2+}$	406	3000	610, 600	578, 568	32, 32
$[(\mathbf{L3})(Ni^{III})_2(\mu\text{-}O)_2]^{2+}$	412	4800	599	570	29
$[(\mathbf{L4})(Ni^{III})_2(\mu\text{-}O)_2]^{2+}$	414	5600	609	579	30
$[(\mathbf{L5})(Ni^{III})_2(\mu\text{-}O)_2]^{2+}$	406	1200	610	577	33

[a] In acetone at −80 °C.

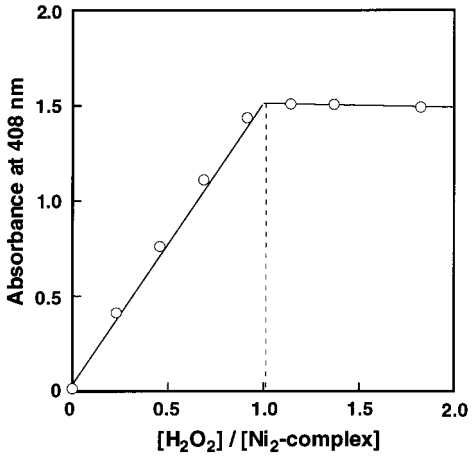

Figure 5. Titration of $[(\mathbf{L1^H}Ni^{II})_2(\mu\text{-}OH)_2](ClO_4)_2$ (2.5×10^{-4} M) with H_2O_2 in acetone at −90 °C.

having a similar absorption band around 400 nm.[38] The same absorption intensity of the LMCT band was obtained even when an excess amount of H_2O_2 was added (see Figure 5), indicating that the stoichiometry of the reaction between H_2O_2 and the bis(μ-hydroxo)dinickel(II) complexes is 1:1. The same 1:1 stoichiometry was obtained in all other cases with **L2**−**L5**.

The intermediates in all cases exhibited a resonance Raman band at 600−610 cm^{-1}, which shifted to 570−580 cm^{-1} when $H_2{}^{16}O_2$ was replaced by $H_2{}^{18}O_2$. In Figure 6 is shown a typical

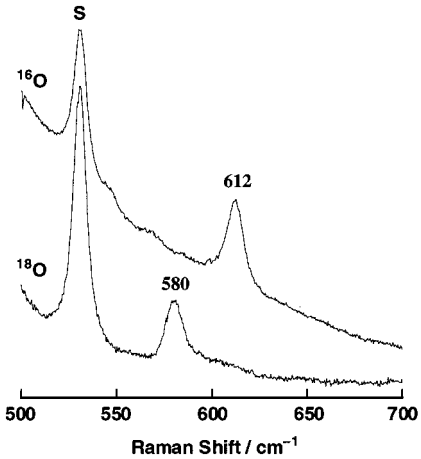

Figure 6. Resonance Raman spectra of $[(\mathbf{L1^H}Ni^{III})_2(\mu\text{-}^{16}O)_2]^{2+}$ and $[(\mathbf{L1^H}Ni^{III})_2(\mu\text{-}^{18}O)_2]^{2+}$ obtained with 406.7 nm excitation in acetone at −80 °C.

example of the spectra obtained with ligand $\mathbf{L1^H}$, and all the resonance Raman data are included in Table 4. The low-frequency resonance Raman bands around 600 cm^{-1} are very similar to those of $[Cu_2(\mu\text{-}O)_2]^{2+}$ complexes (~600 cm^{-1}), and the observed isotope shift of the resonance Raman band ($\Delta\nu$ = ~30 cm^{-1}) agrees well with that observed for bis(μ-oxo)-dicopper(III) complexes.[38,39] It should be noted that the oxygen isotope-sensitive mode of the intermediate supported by **L2** appears as a doublet in the ^{16}O and ^{18}O derivatives, as indicated in Table 4. There may be conformational isomers in this ligand system. The shorter strap (C3) in **L2** may reduce the molecular flexibility to inhibit the interconversion between the two conformational isomers, although their structures remain to be determined. In addition, the intermediates were ESR silent in all cases.

From these spectroscopic characteristics together with the 1:1 stoichiometry between H_2O_2 and the bis(μ-hydroxo)dinickel-(II) complex, the intermediates formed in all the ligand systems are most likely bis(μ-oxo)dinickel(III) complexes as shown in eq 1. In fact, the ESI mass spectrum of an acetone solution containing the intermediate with ligand **L4** showed positive ions with prominent peaks at *m*/*z* 335 and 769, the observed mass values and isotope patterns of which correspond to the $\{[(\mathbf{L4})(Ni^{III})_2(\mu\text{-}O)_2]\}^{2+}$ and $\{[(\mathbf{L4})(Ni^{III})_2(\mu\text{-}O)_2](ClO_4)\}^{+}$ ions, respectively, as shown in Figure 7. Unfortunately, we could not obtain single crystals of the bis(μ-oxo)dinickel(III) complexes despite our great efforts. However, we expect that overall structures of the bis(μ-oxo) complexes are similar to those of the corresponding bis(μ-hydroxo) complexes (Figures 1 and 2), even though the bond lengths of the Ni−O and Ni−N bonds would be shortened due to the higher oxidation state of the nickel ions [Ni(III)].[22,23] It should be emphasized that the bis-(μ-oxo)dinickel(III) complex was similarly obtained in the reaction of the bis(μ-methoxo)dinickel(II) complex of **L4** with H_2O_2 under the same experimental conditions. This result gave us important insight into the mechanism of formation of the bis(μ-oxo) species, as discussed below.

Mechanism of Formation of the Bis(μ-oxo)dinickel(III) Complexes. Bis(μ-hydroxo) dinuclear metal complexes $[M(\mu\text{-}OH)_2M$; M = Cu^{II} and $Ni^{II}]$ have often been utilized as precursors for preparation of the dinuclear (μ-η^2:η^2-peroxo) and bis(μ-oxo) complexes.[6,22,23] To shed light on the mechanism of

(37) Quantitative formation of $[(\mathbf{L5})(Ni^{III})_2(\mu\text{-}O)_2]^{2+}$ has been confirmed by the titration of $[(\mathbf{L5})(Ni^{II})_2(\mu\text{-}OH)_2]^{2+}$ with H_2O_2. The reason for such a small ϵ value of $[(\mathbf{L5})(Ni^{III})_2(\mu\text{-}O)_2]^{2+}$ as compared with those of others is not clear at present.

(38) Henson, M. J.; Mukherjee, P.; Root, D. E.; Stack, T. D. P.; Solomon, E. I. *J. Am. Chem. Soc.* **1999**, *121*, 10332−10345.

(39) Holland, P.; Cramer, C. J.; Wilkinson, E. C.; Mahapatra, S.; Rodger, K. R.; Itoh, S.; Taki, M.; Fukuzumi, S.; Que, L., Jr.; Tolman, W. B. *J. Am. Chem. Soc.* **2000**, *122*, 792−802.

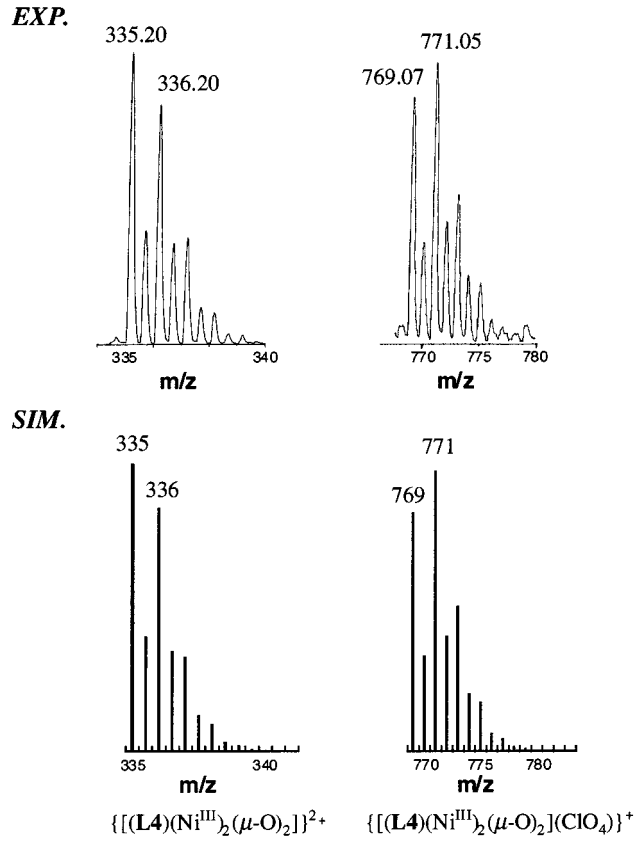

Figure 7. Experimental (top) and calculated (bottom) peak envelopes in the positive-ion electrospray mass spectra of $\{[(\mathbf{L4})(Ni^{III})_2(\mu\text{-}O)_2]\}^{2+}$ and $\{[(\mathbf{L4})(Ni^{III})_2(\mu\text{-}O)_2](ClO_4)\}^{+}$ in acetone.

such reactions, kinetic studies on the reactions between the starting dinickel(II) complexes and H_2O_2 have been performed.

The increase in the absorption band at 408 nm due to $[(\mathbf{L1^H}\text{-}Ni^{III})_2(\mu\text{-}O)_2]^{2+}$ obeyed first-order kinetics, even though an equimolar amount of H_2O_2 was used, as shown in the inset of Figure 4. Moreover, the same first-order rate constants ($k_f = 0.14 \pm 0.02\ s^{-1}$) were obtained for formation of the bis(μ-oxo)-dinickel(III) complex of ligand **L1H** when the concentrations of the starting material, $[(\mathbf{L1^H}Ni^{II})_2(\mu\text{-}OH)_2](ClO_4)_2$, and H_2O_2 were varied {[bis(μ-hydroxo)dinickel(II)] = 1.7×10^{-4}−5.0×10^{-4} M, $[H_2O_2] = 2.5 \times 10^{-4}$−$1.0 \times 10^{-3}$ M}. This indicates that the formation of bis(μ-oxo)dinickel(III) complex is first-order with respect to the starting dinickel(II) complex but zeroth-order on the H_2O_2 concentration. The activation parameters ($\Delta H^{\ddagger}$ and $\Delta S^{\ddagger}$) for the formation process have been determined from the temperature dependence of k_f (−75 to −95 °C). Similar kinetic behavior (first-order kinetics of the intermediate formation and the zeroth-order dependence of k_f on the H_2O_2 concentration) was obtained with other bis(μ-hydroxo)dinickel-(II) complexes and with the bis(μ-methoxo)dinickel(II) complex. The first-order rate constants (k_f) determined at −90 °C and the activation parameters for formation of the bis(μ-oxo)-dinickel(III) complexes are summarized in Table 5.

Table 5. Kinetic Data for the Formation of Bis(μ-oxo)dinickel(III) Intermediate

complex	k_f, s^{-1} [a]	$\Delta H^{\ddagger}$, kcal mol^{-1}	$\Delta S^{\ddagger}$, cal K^{-1} mol^{-1}
$[(\mathbf{L1^H}Ni^{III})_2(\mu\text{-}O)_2]^{2+}$ [b]	0.14	5.6 ± 0.1	−30.9 ± 0.6
$[(\mathbf{L2})(Ni^{III})_2(\mu\text{-}O)_2]^{2+}$ [b]	0.030	9.2 ± 0.3	−14.4 ± 1.5
$[(\mathbf{L3})(Ni^{III})_2(\mu\text{-}O)_2]^{2+}$ [b]	0.000076	12.3 ± 0.4	−9.5 ± 1.8
$[(\mathbf{L4})(Ni^{III})_2(\mu\text{-}O)_2]^{2+}$ [b]	0.0049	9.0 ± 0.3	−18.8 ± 1.8
$[(\mathbf{L4})(Ni^{III})_2(\mu\text{-}O)_2]^{2+}$ [c]	0.0047	10.0 ± 0.3	−17.8 ± 1.5
$[(\mathbf{L5})(Ni^{III})_2(\mu\text{-}O)_2]^{2+}$ [b]	0.046	7.5 ± 0.2	−22.4 ± 1.1

[a] In acetone at −90 °C. [b] Started with the bis(μ-hydroxo)dinickel(II) complex. [c] Started with the bis(μ-methoxo)dinickel(II) complex.

Quantitative formation of ^{18}O-labeled bis(μ-oxo) core in the reaction of the bis(μ-hydroxo)dinickel(II) with $H_2{}^{18}O_2$, demonstrated by the resonance Raman spectrum (Figure 6), clearly indicates that both oxygen atoms of the bis(μ-oxo) complex come from the added H_2O_2. In addition, the same bis(μ-oxo)-dinickel(III) complex was obtained in the reaction of the bis-(μ-methoxo)dinickel(II) with H_2O_2. In the case of the bis(μ-methoxo)dinickel(II) complex, the first-order rate constant for formation of the bis(μ-oxo) complex is also independent of the H_2O_2 concentration.

All these results unambiguously demonstrate that the formation of the bis(μ-oxo)dinickel(III) complex from the bis(μ-hydroxo)- or bis(μ-methoxo)dinickel(II) complex does not proceed *in one step* but involves intermediate(s) during the course of the reaction. Formation of a (μ-η^2:η^2-peroxo)dinickel-(II) intermediate would be plausible, but its rate-limiting decay is unlikely, since accumulation of such an intermediate could not be detected by UV−vis and resonance Raman spectra.[40] One can then assume a mechanism involving a rate-determining isomerization of the bis(μ-hydroxo)- or bis(μ-methoxo)dinickel-(II) complex prior to rapid H_2O_2 attack and decay to the bis-(μ-oxo)dinickel(III) complex, as shown in Scheme 1. The reactivity of the mononucleating ligand system (**L1H**) is much higher than those of the dinucleating ligand systems (**L2**−**L5**), as shown in Table 5. The straps in **L2**−**L5** may inhibit the isomerization process as compared to the more flexible mononucleating system **L1H**. This is reflected in the larger $\Delta H^{\ddagger}$ values of the dinucleating ligand systems (see Table 5).[41]

Scheme 1

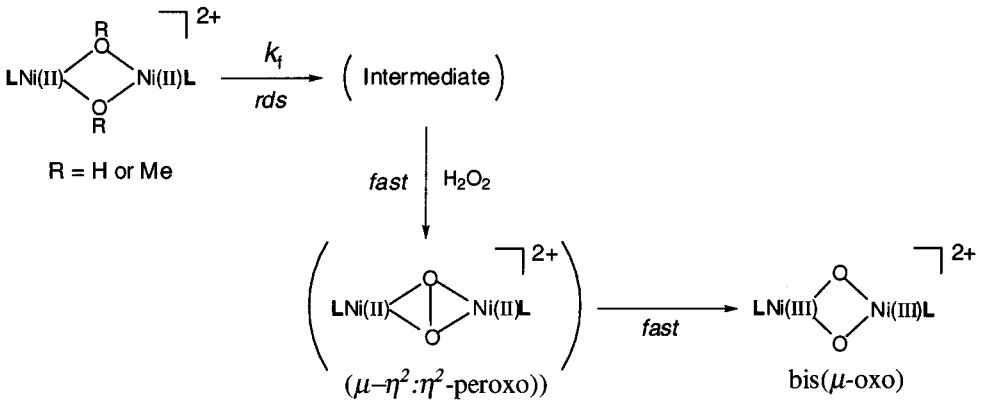

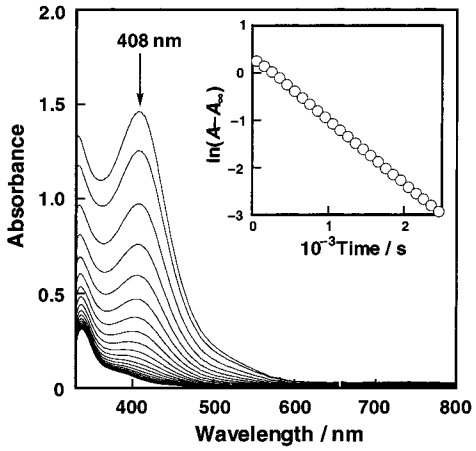

Figure 8. Spectral change for the benzylic ligand hydroxylation in $[(\mathbf{L1^H}Ni^{III})_2(\mu\text{-}O)_2](ClO_4)_2$ (2.5×10^{-4} M) in acetone at −30 °C. Inset: First-order plot based on the absorption change at 408 nm.

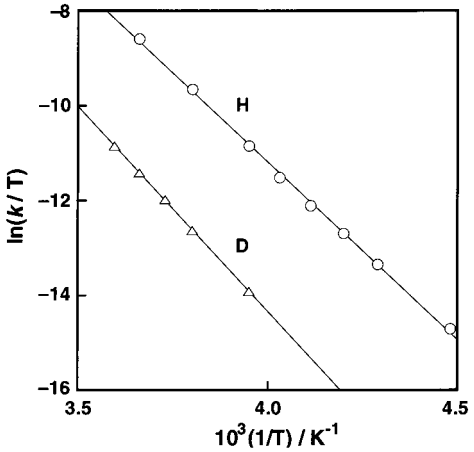

Figure 9. Eyring plots for the ligand hydroxylation process of $[(\mathbf{L1^H}\text{-}Ni^{III})_2(\mu\text{-}^{16}O)_2]^{2+}$ (line H) and $[(\mathbf{L1^H}\text{-}d_4Ni^{III})_2(\mu\text{-}^{16}O)_2]^{2+}$ (line D) in acetone.

Chart 2

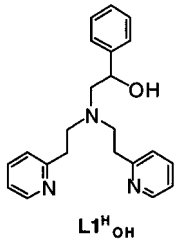

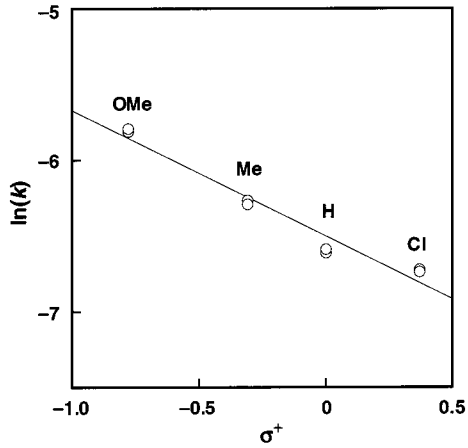

Figure 10. Hammett plot for the decomposition of $[(\mathbf{L1^X}Ni^{III})_2(\mu\text{-}O)_2]^{2+}$ (X = MeO, Me, H, Cl) in acetone at −30 °C. The line represents a least-squares fit to the data ($r = 0.98$) with the slope of $\rho = -0.83$.

It is interesting to note that the nickel(II) complexes afford only bis(μ-oxo)dinickel(III) complexes, whereas the copper(II) complexes supported by the same ligands predominantly gave the (μ-η^2:η^2-peroxo)dicopper(II) species in the reaction with H_2O_2.[30b,42,43] Thus, it is obvious that the metal ion plays a critical role in enhancing the O−O bond homolysis of the peroxo species, although the origin of such a difference remains to be clarified.

Aliphatic Ligand Hydroxylation in the Bis(μ-oxo)dinickel-(III) Complex. The bis(μ-oxo)dinickel(III) complex supported by $\mathbf{L1^H}$ is fairly stable at a low temperature (below −80 °C) but gradually decomposes at a higher temperature (above −50 °C), as shown in Figure 8. Product analysis of the final reaction mixture revealed that hydroxylation at the benzylic position of the ligand side arm occurred to give $\mathbf{L1^H_{OH}}$ (Chart 2), as reported for the reaction of $[Cu^I(\mathbf{L1^H})]^+$ with O_2.[30] The isolated yield of the hydroxylated product was 48% based on the ligand used. Since the bis(μ-oxo) core has two ligand molecules, the yield of hydroxylation is 96% based on the bis(μ-oxo) core.

The oxygen source of the OH group in $\mathbf{L1^H_{OH}}$ has been confirmed as hydrogen peroxide by the isotope labeling experiment using $H_2{}^{18}O_2$. The resonance Raman spectra obtained using $H_2{}^{18}O_2$ at −80 °C (Figure 6) have confirmed that ^{18}O is quantitatively incorporated into the bis(μ-oxo)dinickel(III) core at the low temperature. In the product analysis using $H_2{}^{18}O_2$ at a higher temperature (−20 °C), however, only 72% of ^{18}O is incorporated into the hydroxylated ligand $\mathbf{L1^H_{OH}}$. Thus, the oxygen atom of the bis(μ-oxo)dinickel(III) core is exchangeable with that of H_2O at the higher temperature. Que and co-workers also reported that the oxygen atom of Fe(III)(μ-O)$_2$Fe(IV) core was easily replaced by that of H_2O.[24] It should be noted, however, that the oxygen exchange rate of our bis(μ-oxo)-dinickel(III) core is significantly slower than those of the bis-(μ-oxo)dinickel(III) complexes of Hikichi and co-workers[22] and Suzuki and co-workers.[23] They reported that the Raman peak corresponding to the Ni−^{18}O stretching in their bis(μ-oxo) diamond core was hardly observed because of the rapid exchange between ^{16}O and ^{18}O.[22,23]

The ligand hydroxylation process obeyed first-order kinetics, as shown in the inset of Figure 8. From the temperature dependence of the decay rate (k_d) (Eyring plot, Figure 9; line H) were obtained the activation parameters $\Delta H_H^{\ddagger} = 14.3 \pm 0.2$ kcal mol^{-1} and $\Delta S_H^{\ddagger} = -12.5 \pm 0.7$ cal K^{-1} mol^{-1}. Perdeuteration of the ligand side arm ($\mathbf{L1^H}$-d_4; 1,1,2,2-tetra-deuterated phenethylamine derivative) resulted in a significant decrease in the decay rate, as shown in Figure 9, where the activation parameters were determined to be $\Delta H_D^{\ddagger} = 17.2 \pm 0.1$ kcal mol^{-1} and $\Delta S_D^{\ddagger} = -7.0 \pm 0.4$ cal K^{-1} mol^{-1} from the Eyring plot (line D). The ^{1}H NMR spectrum of the organic product showed that the ethylene group of the pyridine side arms remained intact after the ligand hydroxylation of $\mathbf{L1^H}$-d_4. A very large kinetic deuterium isotope effect was obtained for the hydroxylation reaction (e.g., KIE = 21.4 at −20 °C). Such

(40) Although a (μ-η^2:η^2-peroxo)dinickel(II) complex is not known, it may have UV−vis and resonance Raman spectra similar to those of the (μ-η^2:η^2-peroxo)dicopper(II) complexes.

(41) The small $\Delta H^{\ddagger}$ value is partially compensated with the most negative $\Delta S^{\ddagger}$ value for the mononucleating ligand (**L1H**).

(42) Pidcock, E.; Obias, H. V.; Abe, M.; Liang, H.-C.; Karlin, K. D.; Solomon, E. I. *J. Am. Chem. Soc.* **1999**, *121*, 1299−1308.

(43) Pidcock, E.; Obias, H. V.; Zhang, C. X.; Karlin, K. D.; Solomon, E. I. *J. Am. Chem. Soc.* **1998**, *120*, 7841−7847.

Scheme 2

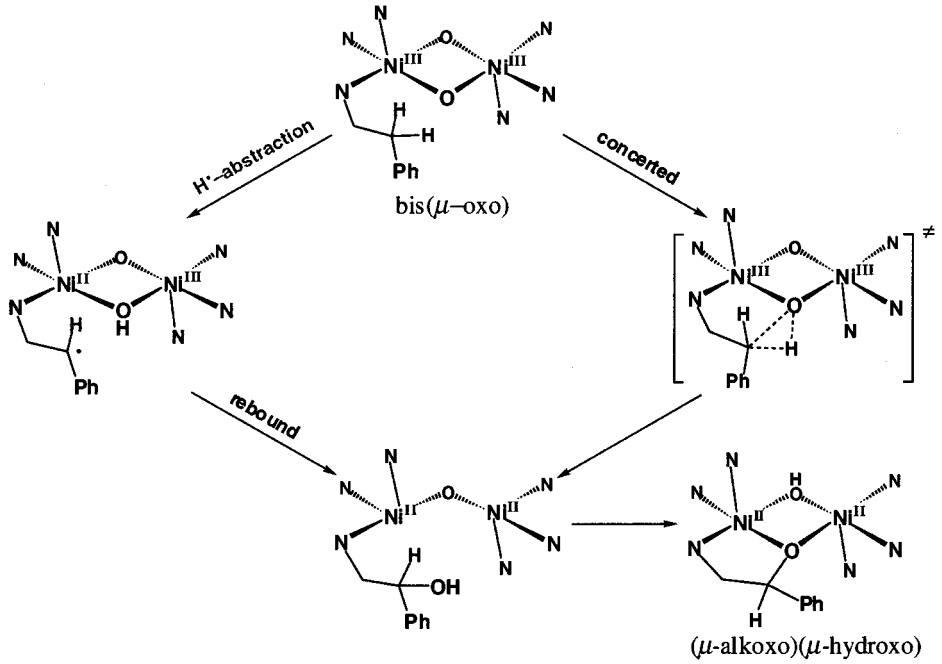

a large primary kinetic isotope effect suggests the occurrence of tunneling for the hydrogen atom abstraction. The criteria to be applied for detection of tunneling depend on accurate measurement of k_H/k_D as a function of temperature. Since it is the curvature of the Arrhenius plot which demonstrates experimentally the involvement of tunneling, the apparent activation parameters for the tunneling hydrogen transfer, derived from linear Arrhenius plots in the normal range of measurement, would be $\Delta H_H^{\ddagger} - \Delta H_D^{\ddagger} > 1.4$ kcal mol^{-1} and $\Delta S_H^{\ddagger} - \Delta S_D^{\ddagger} > 1$ cal K^{-1} mol^{-1}.[44] These criteria are met in the present case: $\Delta H_H^{\ddagger} - \Delta H_D^{\ddagger} = 4.7$ kcal mol^{-1} and $\Delta S_H^{\ddagger} - \Delta S_D^{\ddagger} = 5.5$ cal K^{-1} mol^{-1}.

Examination of the para substituent effects using **L1^X** (Hammett plot of k_d vs σ^+) gave $\rho = -0.83$ ($r = 0.98$), as shown in Figure 10. The ρ value is nearly the same as those reported for the aliphatic ligand hydroxylation in [**L^{py1}**(Cu)$_2$-(μ-O)$_2$]$^{2+}$ ($\rho = -1.48$, **L^{py1}** = *N*-[(2-(2-pyridyl)ethyl)-2-(para-substituted-phenyl)ethylamine])[26] and for the oxidative *N*-dealkylation in [(**L$^{(p-R)Bn3}$**Cu)$_2$(μ-O)$_2$]$^{2+}$ ($\rho = -0.8$, **L$^{(p-R)Bn3}$** = 1,4,7-tri(para-substituted-benzyl)triazacyclononane),[25] where hydrogen atom abstraction by the bis(μ-oxo) complex is the rate-determining step. Thus, ligand hydroxylation by the bis(μ-oxo)dinickel(III) core may proceed via the rate-determining hydrogen atom abstraction (k_d) followed by hydroxyl rebound or its concerted variant as proposed in the copper system (Scheme 2).[26]

The occurrence of tunneling in hydrogen atom abstraction by the bis(μ-oxo)dinickel(III) complex is in sharp contrast with the aliphatic ligand hydroxylation of the corresponding active oxygen copper complex, in which only a small k_H/k_D value (1.8 at −40 °C) is obtained.[30b] In the case of the copper system, only the (μ-η^2:η^2-peroxo)dicopper(II) complex is observable as an intermediate, and O−O bond homolysis of the peroxo complex to give the corresponding bis(μ-oxo)dicopper(III) complex is the rate-determining step for the overall aliphatic ligand hydroxylation reaction.[30b] The subsequent hydrogen atom abstraction process by the bis(μ-oxo)dicopper(III) complex is too fast to be the rate-determining step. This is the reason for the small kinetic isotope effects and the absence of para substituent effects on the overall ligand hydroxylation reaction by the (μ-η^2:η^2-peroxo)dicopper(II) complex.[30b]

Table 6. Kinetic Data for the Oxidation of External Substrates by the Bis(μ-oxo)dinickel(III) [(**L1^H**Ni^{III})$_2$(μ-O)$_2$]$^{2+}$ Complex in Acetone

substrate	k_2, M^{-1} s^{-1} [a]	$\Delta H^{\ddagger}$, kcal mol^{-1}	$\Delta S^{\ddagger}$, cal K^{-1} mol^{-1}
2,4-di-*tert*-butylphenol	1.08	9.1 ± 0.1	−9.7 ± 0.5
2,6-di-*tert*-butylphenol	1.66×10^{-2}	9.8 ± 0.5	−14.4 ± 2.4
1,4-cyclohexadiene	1.19×10^{-1}	5.3 ± 0.3	−31.0 ± 1.6

[a] At −50 °C.

The bis(μ-oxo)dinickel(III) complexes of **L2**−**L4** are also stable at low temperature (−80 °C) but gradually decompose at a higher temperature. The k_d values (first-order rate constant of the self-decomposition) at −20 °C in acetone are 4.6×10^{-3}, 9.9×10^{-4}, and 1.6×10^{-4} s^{-1} for the bis(μ-oxo)dinickel(III) complexes with **L2**, **L3**, and **L4**, respectively. The k_d value of [(**L2**)Ni^{III}]$_2$(μ-O)$_2$]$^{2+}$ is comparable to the value of [(**L1^H**Ni^{III})$_2$-(μ-O)$_2$]$^{2+}$ ($k_d = 4.9 \times 10^{-3}$ s^{-1}) under the same experimental conditions (−20 °C in acetone), whereas the stability of the bis(μ-oxo)dinickel(III) core is significantly enhanced when the alkyl strap of the dinucleating ligand is elongated (C4 to C5).[45]

Oxidation of External Substrates. The reactivity for hydrogen atom abstraction of the bis(μ-oxo)dinickel(III) complex has also been demonstrated by the reaction with external substrates such as 2,4-di-*tert*-butylphenol, 2,6-di-*tert*-butylphenol, and 1,4-cyclohexadiene. The oxidation of these substrates by [(**L1^H**Ni^{III})$_2$(μ-O)$_2$]$^{2+}$ was examined in a temperature range from −50 to −70 °C, where the rates of the self-decomposition (ligand hydroxylation) were negligible (only 10^{-2}−10^{-4} times) as compared with the rates of oxidation of the external substrates. Those substrates were readily oxidized in acetone to the corresponding diphenol derivatives and benzene, respectively. In this case, the original ligand was recovered almost

(44) Kwart, H. *Acc. Chem. Res.* **1982**, *15*, 401−408.

(45) ^{1}H NMR and MS analysis of the organic products obtained after the workup treatment of the reaction with ligand **L4** indicated that some of the ligand was hydroxylated at its alkyl strap moiety (∼50% yield), although the product mixture is not so simple.

Scheme 3

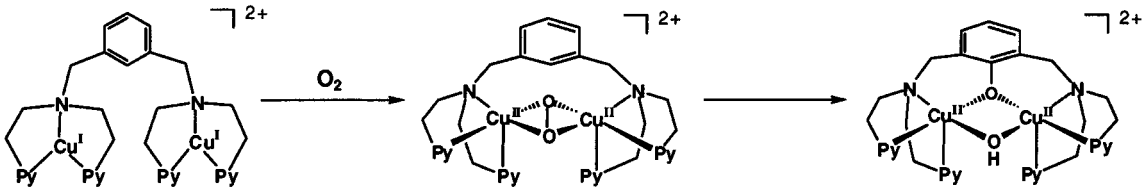

$(\mu\text{-}\eta^2\text{:}\eta^2\text{-peroxo})(Cu^{II})_2$

Scheme 4

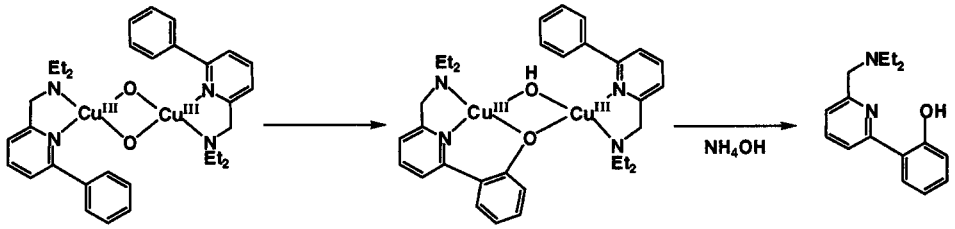

bis$(\mu\text{-oxo})(Cu^{III})_2$

Scheme 5

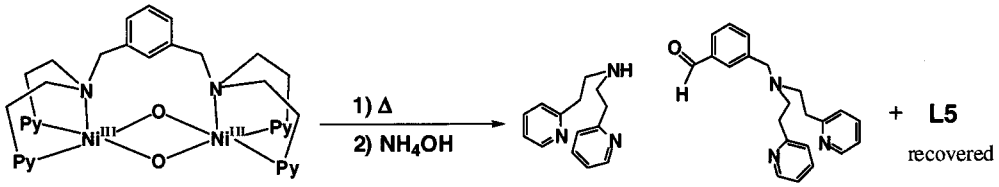

$[(\mathbf{L5})(Ni^{III})_2(\mu\text{-}O)_2]^{2+}$

quantitatively after the reaction with the external substrates without ligand hydroxylation. On the other hand, triphenylphosphine and thioanisole were not oxidized under such conditions. The reactions were followed by monitoring a decrease of the absorption band (408 nm) due to the bis(μ-oxo)dinickel(III) intermediates, which obeyed pseudo-first-order kinetics in the presence of a large excess of substrate. Plots of the pseudo-first-order rate constants k_{obs} against the substrate concentrations gave straight lines passing through the origin, demonstrating that the reactions were first-order with respect to substrate. Arrhenius plots of the second-order rate constants k_2 (the slope of the linear plot of k_{obs} vs [substrate]) then gave the activation parameters ($\Delta H^{\ddagger}$ and $\Delta S^{\ddagger}$), as summarized in Table 6. The overall reactivity of the substrate is mainly governed by the activation entropy ($\Delta S^{\ddagger}$). This indicates that the transition state of the hydrogen atom abstraction by the bis(μ-oxo) species requires a highly ordered geometry. Thus, the phenol derivatives having the $-$OH group with higher flexibility is more reactive than 1,4-cyclohexadiene, in which $-$C$-$H bond mobility is rather restricted.

Reactivity of the Bis(μ-oxo)dinickel(III) Complex Supported by L5. In the pioneering work by Karlin and co-workers in Cu/O_2 chemistry, aromatic ligand hydroxylation in $[Cu^{I}_2(\mathbf{L5})]^{2+}$ by O_2 was first reported in the early 1980s (Scheme 3).[33,46] Mechanistic studies have indicated that the aromatic hydroxylation reaction involves electrophilic attack on the arene ring by a (μ-η^2:η^2-peroxo)dicopper(II) intermediate as a key step.[42,47] Since this reaction is an arene hydroxylation by O_2 at a distinct dinuclear copper(I) site involving a side-on-type peroxo species, it can serve as a functional model of tyrosinase.[48] On the other hand, however, more recent studies in Cu/O_2 chemistry have clearly shown that the O$-$O bond homolysis takes place from the (μ-η^2:η-peroxo)dicopper(II) complex to provide a bis(μ-oxo)dicopper(III) species and that the equilibrium position between the peroxo and bis(μ-oxo) complexes is largely controlled by the supported ligands and solvents.[13] The bis(μ-oxo)dicopper(III) species has been shown to exhibit an ability to undergo not only hydrogen atom abstraction of the phenols but also C$-$H bond activation of the alkyl side chain of the ligands.[25,26] Furthermore, Tolman et al. have recently demonstrated that the bis(μ-oxo)dicopper(III) complex can hydroxylate an aromatic ring, suggesting a possible contribution of the bis(μ-oxo)dicopper(III) intermediate in the tyrosinase reaction (Scheme 4).[49] Thus, it is worth investigating the reactivity of $[(\mathbf{L5}Ni^{III})_2(\mu\text{-}O)_2]^{2+}$ in comparison with that of the corresponding dicopper complex.

The bis(μ-oxo)dinickel(III) complex supported by the dinucleating ligand **L5** gradually decomposed at -30 °C in acetone as in the case of $[(\mathbf{L1}^{X}Ni^{III})_2(\mu\text{-}O)_2]^{2+}$. The decay of the absorption band at 406 nm due to $[(\mathbf{L5})(Ni^{III})_2(\mu\text{-}O)_2]^{2+}$ obeyed first-order kinetics, suggesting the decomposition is also a unimolecular process. From the Eyring plot are obtained the activation parameters as $\Delta H_H^{\ddagger} = 12.8 \pm 0.1$ kcal mol^{-1} and $\Delta S_H^{\ddagger} = -17.3 \pm 0.4$ cal K^{-1} mol^{-1}. The $\Delta H^{\ddagger}$ and $\Delta S^{\ddagger}$ values are fairly similar to those for the aliphatic ligand hydroxylation reactions of $[(\mathbf{L1}^{H}Ni^{III})_2(\mu\text{-}O)_2]^{2+}$.

Product analysis of the decomposition of $[(\mathbf{L5})(Ni^{III})_2(\mu\text{-}O)_2]^{2+}$ was performed by extracting the metal ions from the complex with aqueous NH_3 solution. The ^{1}H NMR spectrum

(46) Karlin, K. D.; Dahlstrom, P. L.; Cozzette, S. N.; Scensny, P. M.; Zubieta, J. *J. Chem. Soc., Chem. Commun.* **1981**, 881$-$882.

(47) Nasir, M. S.; Cohen, B. I.; Karlin, K. D. *J. Am. Chem. Soc.* **1992**, *114*, 2482$-$2494.

(48) Solomon, E. I.; Sundaram, U. M.; Machonkin, T. E. *Chem. Rev.* **1996**, *96*, 2563$-$2605.

(49) Holland, P. L.; Rodgers, K. R.; Tolman, W. B. *Angew. Chem.* **1999**, *111*, 1210$-$1213; *Angew. Chem., Int. Ed.* **1999**, *38*, 1139$-$1142.

Scheme 6

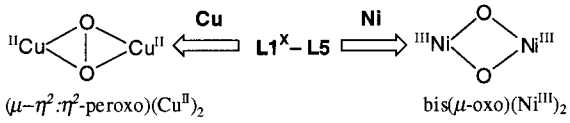

of the organic product clearly showed that no aromatic hydroxylation product was formed but that oxidative *N*-dealkylation occurred in 30% yield (see Experimental Section), as shown in Scheme 5. This result shows a sharp contrast with the corresponding copper system supported by the same ligand **L5**, where quantitative aromatic ligand hydroxylation occurred (Scheme 3). As mentioned above, the aromatic hydroxylation of the copper system has been proposed to involve the (μ-η^2:η^2-peroxo)dicopper(II) complex as the actual active species.[42] Thus, the bis(μ-oxo)dinickel(III) complex has no ability to undergo aromatic hydroxylation, but instead it exhibits reactivity for hydrogen atom abstraction from activated C−H bonds (benzylic hydrogen).

Summary and Conclusions

As demonstrated so far, nickel ion strongly enhances the O−O bond homolysis of the peroxo intermediate to produce the bis(μ-oxo)dinickel(III) complex, in contrast with copper ion, which forms a relatively stable (μ-η^2:η^2-peroxo) species with the same ligands (Scheme 6). Theoretical studies on the copper systems have suggested that the thermal stabilities of the (μ-η^2:η^2-peroxo)dicopper(II) and the bis(μ-oxo)dicopper(III) cores are comparable.[50,51] Thus, the equilibrium position between them is largely determined by the ligands, solvents, and counteranions used.[13,27b] In this context, the steric bulkiness of the alkyl substituent (R) of the bis[2-(2-pyridyl)ethyl]amine ligand [RN($CH_2CH_2Py)_2$] is an important factor that controls the equilibrium position between the (μ-η^2:η^2-peroxo)dicopper(II) and the bis(μ-oxo)dicopper(III), since only the (μ-η^2:η^2-peroxo) species was detected by resonance Raman spectroscopy in the cases of **L1^H** (R = CH_2CH_2Ph)[30b] and **L2**−**L5**,[42,43] while a mixture of the (μ-η^2:η^2-peroxo)dicopper(II) and the bis(μ-oxo)dicopper(III) complexes was obtained by using the ligand with a smaller alkyl substituent (R = Me).[51] In the case of nickel complexes, all the RN($CH_2CH_2Py)_2$-type ligands afford only the bis(μ-oxo)dinickel(III) isomer, implying that the bis(μ-oxo)dinickel(III) core is much more stable than the (μ-η^2:η^2-peroxo)dinickel(II) core.

The bis(μ-oxo)dinickel(III) complexes undergo aliphatic ligand hydroxylation like the bis(μ-oxo)dicopper(III) complexes. The bis(μ-oxo)dinickel(III) unit also acts as a hydrogen atom acceptor from external substrates such as phenols and 1,4-cyclohexadiene, whereas the bis(μ-oxo)dicopper(III) unit itself exhibits no reactivity toward 1,4-cyclohexadiene.[27a,52] Thus, the nickel complex has a higher reactivity toward *aliphatic C−H bond activation* as compared with the copper complex. On the other hand, however, the bis(μ-oxo)dinickel(III) complex does not show any reactivity toward aromatic hydroxylation (Scheme 5) nor oxygen atom transfer to phosphines and sulfides. The origin of such a sharp contrast with regard to both the thermal stability and the reactivity between the nickel and the copper systems found in this study remains to be clarified in the future.

Experimental Section

General. All chemicals used in this study except the ligands and the complexes were commercial products of the highest available purity and were further purified by the standard methods, if necessary.[53] Ligands **L1^X** and **L2**−**L5** were prepared according to the reported procedures.[30−33] ^{18}O-Labeled hydrogen peroxide $H_2{}^{18}O_2$ was prepared according to the reported procedure.[54] FT-IR spectra were recorded with a Shimadzu FTIR-8200PC. UV−vis spectra were measured using a Hewlett-Packard HP8452 or a Hewlett-Packard HP8453 diode array spectrophotometer with a Unisoku thermostated cell holder designed for low-temperature measurements. Ordinary mass spectra were recorded with a JEOL JNX-DX303 HF mass spectrometer. ESI−MS (electrospray ionization mass spectra) measurements were performed on a JEOL JMS-700T tandem MS station or a PE SCIEX API 150EX. ^1H NMR spectra were recorded on a JEOL FT-NMR GX-400 spectrometer. ESR measurements were performed on a JEOL JES-ME-2X spectrometer at −196 °C (liquid N_2 temperature).

The cyclic voltammetry (CV) measurements were performed on a BAS 100B or an ALS 600 electrochemical analyzer in anhydrous acetone containing 0.01 M $NBu_4(ClO_4)$ as supporting electrolyte. The Pt working electrodes were polished with a polishing alumina suspension and rinsed with acetone before use. The counter electrode was a Pt wire. A silver pseudo-reference electrode was used, and the potentials were determined using the ferrocene/ferricenium (Fc/Fc^+) couple as a reference. All electrochemical measurements were carried out at 25 °C under an atmospheric pressure of nitrogen.

Resonance Raman Measurements. The 406.7 nm line of a Kr^+ laser (model 2060, Spectra Physics) was used as the exciting source. Visible resonance Raman scattering was detected with a liquid-nitrogen-cooled CCD detector (model LN/CCD-1340 (400PB, Princeton Instruments) attached to a 1 m single polychlomator (model MC-100DG, Ritsu Oyo Kogaku). The mechanical slit width and slit height were set to be 200 μm and 20 mm, respectively. The spectral slit width was 2.1 cm^{-1}. A wavenumber per one channel was 0.4 cm^{-1}. The laser power used was 6.5 or 2.7 mW at the sample point. All measurements were carried out at −80 °C with a spinning cell (1000 rpm). Raman shifts were calibrated with indene, and the accuracy of the peak positions of the Raman bands was ±1 cm^{-1}.

Synthesis of Bis(μ-hydroxo)dinickel(II) Complexes. To a stirred solution of the ligand (0.5 mmol) in ethanol (10 mL) was added dropwise a solution of $Ni(ClO_4)_2{\cdot}6H_2O$ (0.5 mmol) in ethanol (10 mL). The mixture became a suspension for a while, but it became a clean solution after further stirring. When the suspended material did not dissolve into the solution, a small amount of acetonitrile was added. The solution was then stirred under Ar for 10 min. Addition of triethylamine (0.5 mmol) dissolved in ethanol into the solution resulted in precipitation of green microcrystals. Slow addition of ether into the supernatant further gave the green microcrystals of the bis(μ-hydroxo)dinickel(II) complexes. The precipitated material was isolated by filtration and dried in vacuo for 30 min. Isolated yields and analytical data of the nickel complexes are presented below. All bis(μ-hydroxo)dinickel(II) complexes were ESR silent and gave significantly broadened ^1H NMR spectra.

[($L^{OMe}Ni^{II}$)$_2$(μ-OH)$_2$](ClO_4)$_2{\cdot}H_2O$: emerald green color; 62% yield; FT-IR (KBr) 3643 cm^{-1} (μ-OH), 1090 and 623 cm^{-1} (ClO_4^-). Anal. Calcd for $C_{46}H_{58}Ni_2N_6O_{13}Cl_2$: C, 50.62; H, 5.36; N, 7.70. Found: C, 50.28; H, 5.30; N, 7.50.

[($L^{Me}Ni^{II}$)$_2$(μ-OH)$_2$](ClO_4)$_2{\cdot}H_2O$: emerald green color; 60% yield; FT-IR (KBr) 3608 cm^{-1} (μ-OH), 1090 and 623 cm^{-1} (ClO_4^-). Anal.

(50) (a) Cramer, C. J.; Smith, B. A.; Tolman, W. B. *J. Am. Chem. Soc.* **1996**, *118*, 11283−11287. (b) Berces, A. *Inorg. Chem.* **1997**, *36*, 4831−4837. (c) Yoshizawa, K.; Ohta, T.; Yamabe, T. *Bull. Chem. Soc. Jpn.* **1997**, *70*, 1911−1917. (d) Liu, X.-Y.; Palacios, A. A.; Novoa, J. J.; Alvarez, S. *Inorg. Chem.* **1998**, *37*, 1202−1212.

(51) (a) Obias, H. V.; Lin, Y.; Murthy, N. N.; Pidcock, E.; Solomon, E. I.; Ralle, M.; Blackburn, N. J.; Neuhold, Y.-M.; Zuberbühler, A. D.; Karlin, K. D. *J. Am. Chem. Soc.* **1998**, *120*, 12960−12961. (b) Pidcock, E.; DeBeer, S.; Obias, H. V.; Hedman, B.; Hodgson, K. O.; Karlin, K. D.; Solomon, E. I. *J. Am. Chem. Soc.* **1999**, *121*, 1870−1878.

(52) Oxidation of 1,4-cyclohexadiene with a bis(μ-oxo)dicopper(III) complex has been recently reported (Taki, M.; Itoh, S.; Fukuzumi, S. *J. Am. Chem. Soc.* **2001**, *123*, 6203−6204). In this case, however, kinetic results have indicated that the bis(μ-oxo)dicopper(III) complex is not the actual active species for the C−H bond activation of the substrate.

(53) Perrin, D. D.; Armarego, W. L. F.; Perrin, D. R. *Purification of Laboratory Chemicals*, 4th ed.; Pergamon Press: Elmsford, NY, 1996.

(54) Sitter, A. J.; Terner, J. *J. Label. Comput. Radiopharm.* **1985**, *22*, 461−465.

Calcd for $C_{46}H_{58}Ni_2N_6O_{11}Cl_2$: C, 52.15; H, 5.52; N, 7.94. Found: C, 52.35; H, 5.42; N, 7.66.

[($L^{H}Ni^{II}$)$_2$(μ-OH)$_2$](ClO$_4$)$_2$·H$_2$O·MeCN: emerald green color; 80% yield; FT-IR (KBr) 3604 cm^{-1} (μ-OH), 1090 and 623 cm^{-1} (ClO_4^-). Anal. Calcd for $C_{46}H_{57}Ni_2N_7O_{11}Cl_2$: C, 51.52; H, 5.36; N, 9.15. Found: C, 51.66; H, 5.18; N, 9.65.

[($L^{Cl}Ni^{II}$)$_2$(μ-OH)$_2$](ClO$_4$)$_2$·H$_2$O: emerald green color; 80% yield; FT-IR (KBr) 3614 cm^{-1} (μ-OH), 1090 and 623 cm^{-1} (ClO_4^-). Anal. Calcd for $C_{44}H_{52}Ni_2N_6O_{11}Cl_4$: C, 48.03; H, 4.76; N, 7.64. Found: C, 47.81; H, 4.65; N, 7.16.

[(L2)(Ni^{II})$_2$(μ-OH)$_2$](ClO$_4$)$_2$·H$_2$O: emerald green color; 72% yield; FT-IR (KBr) 3600 cm^{-1} (μ-OH), 1090 and 624 cm^{-1} (ClO_4^-). Anal. Calcd for $C_{31}H_{42}Ni_2N_6O_{11}Cl_2$: C, 43.14; H, 4.91; N, 9.74. Found: C, 43.41; H, 4.66; N, 9.67.

[(L3)(Ni^{II})$_2$(μ-OH)$_2$](ClO$_4$)$_2$·H$_2$O: light blue color; 65% yield; FT-IR (KBr) 3597 cm^{-1} (μ-OH), 1091 and 623 cm^{-1} (ClO_4^-). Anal. Calcd for $C_{32}H_{44}Ni_2N_6O_{11}Cl_2$: C, 43.82; H, 5.06; N, 9.58. Found: C, 43.82; H, 4.78; N, 9.42.

[(L4)(Ni^{II})$_2$(μ-OH)$_2$](ClO$_4$)$_2$·H$_2$O: green color; 49%; FT-IR (KBr) 3593 cm^{-1} (μ-OH), 1099 and 623 cm^{-1} (ClO_4^-). Anal. Calcd for $C_{36}H_{46}Ni_2N_6O_{12}Cl_2$: C, 44.48; H, 5.20; N, 9.43. Found: C, 44.31; H, 4.87; N, 9.20.

[(L5)(Ni^{II})$_2$(μ-OH)$_2$](ClO$_4$)$_2$·H$_2$O: light blue color; 58% yield; FT-IR (KBr) 3614 cm^{-1} (μ-OH), 1091 and 624 cm^{-1} (ClO_4^-). Anal. Calcd for $C_{36}H_{46}Ni_2N_6O_{12}Cl_2$: C, 45.85; H, 4.92; N, 8.91. Found: C, 45.60; H, 4.58; N, 8.80.

[(L4)(Ni^{II})$_2$(μ-OMe)$_2$](ClO$_4$)$_2$·MeCN·MeOH was obtained when [(**L4**)(Ni^{II})$_2$(μ-OH)$_2$](ClO$_4$)$_2$·H$_2$O was recrystallized from a 1:1 mixture of MeOH and MeCN: green color; 30%; FT-IR (KBr) 1090 and 623 cm^{-1} (ClO_4^-). Anal. Calcd for $C_{38}H_{55}Ni_2N_7O_{11}Cl_2$: C, 46.85; H, 5.69; N, 10.06. Found: C, 46.57; H, 5.20; N, 9.69.

Ligand Hydroxylation (Product Analysis). Typically, bis(μ-hydroxo)dinickel(II) complex (0.10 mmol) was dissolved into deaerated acetone (5 mL), and the solution was further deaerated by bubbling Ar for 10 min. The acetone solution was cooled to −78 °C using a dry ice/acetone bath, to which H_2O_2 (0.10 mmol) was added. The resulting dark brown solution was stirred for several minutes at −78 °C, and then the solution was gradually warmed to −20 °C and stirred at this temperature until the brown color disappeared. A mixture of organic products derived from the ligand was obtained after an ordinary workup treatment with aqueous NH_4OH and following extraction by CH_2Cl_2. Identification of the oxygenated ligand was carried out by comparing the ^{1}H NMR peaks of the product mixture to those of the authentic sample obtained in the previous study.[30b] The yield of the ligand hydroxylation was determined to be 48 ± 2% (96% based on the dinickel complex) by using an integral ratio in the ^{1}H NMR spectrum between the methine proton (−C*H*OH−) of $\mathbf{L^X_{OH}}$ and the pyridine protons at the 6-position from both $\mathbf{L^X_{OH}}$ and $\mathbf{L^X}$. In the self-decomposition of [(**L5**)(Ni^{III})$_2$(μ-O)$_2$]$^{2+}$, ^{1}H NMR and MS analyses of the organic product obtained after the same workup treatment indicated that there was no hydroxylated product at its aromatic ring,[47] but instead the benzaldehyde derivative shown in Scheme 5 and bis[2-(2-pyridyl)-ethyl]amine were detected by GC−MS and ^{1}H NMR (δ = 9.87 for −C*H*O, 30% yield).

The isotope labeling experiment was performed using $H_2{}^{18}O_2$ (85 mM) instead of 30% $H_2{}^{16}O_2$, and the ratio of ^{16}O:^{18}O in the hydroxylated product ($\mathbf{L^H_{OH}}$) was determined to be 72:28 by MS.

Kinetic Measurements. The reaction of the bis(μ-hydroxo)dinickel-(II) complex and H_2O_2 was carried out in a 1 cm path length UV−vis cell that was held in a Unisoku thermostated cell holder designed for low-temperature measurements (a desired temperature can be fixed within ±0.5 °C). After the deaerated solution of the nickel complex (2.5×10^{-4} M) in the cell was kept at the desired temperature for several minutes, an equimolar amount of H_2O_2 (10 μL of a 75 mM acetone solution of H_2O_2) was added from a microsyringe. Rate constants for the formation and decay (ligand hydroxylation) of the bis(μ-oxo)dinickel(III) intermediate were determined by monitoring the increase and decrease in the absorbance at 408 nm.

Oxidation of the external substrates by [($\mathbf{L1^H}$Ni^{III})$_2$(μ-O)$_2$]$^{2+}$ was started by adding the substrate with use of a microsyringe into the solution at a desired temperature (−50 to −70 °C) when the absorption of the bis(μ-oxo)dinickel(III) complex (408 nm) reached a maximum. The reaction was followed by monitoring a decrease in absorbance at 408 nm. Nearly quantitative formation of the oxidation products (diphenol derivatives and benzene) was confirmed by GC−MS.

Titration of the bis(μ-hydroxo)dinickel(II) complex (0.25 mM) with H_2O_2 was performed in a 1 cm path length UV−vis cell at −80 °C. The absorbance at 408 nm determined after a few minutes of each addition of 0.20 equiv of H_2O_2 in acetone (15 mM) was plotted against the molar ratio of [H_2O_2]/[bis(μ-hydroxo)dinickel(II)].

Acknowledgment. This work was partially supported by Grants-in-Aid for Scientific Research Priority Area (Nos. 11228205 and 11228206) and Grants-in-Aid for Scientific Research (Nos. 11440197, 12874082, and 13480189) from the Ministry of Education, Culture, Sports, Science, and Technology, Japan. K.D.K acknowledges support from the National Institutes of Health, USA (GM 28962). The authors also thank Rika Miyake of Osaka City University for her help in the measurement of low-temperature ESI-MS.

Supporting Information Available: Details about the X-ray structure determination including crystallographic data (Figures S1 and S2) and resonance Raman spectra of the bis(μ-oxo)-dinickel(III) complexes supported by **L2**−**L5** (Figures S3−S6) (PDF). X-ray crystallographic data in CIF format are also available. This material is available free of charge via the Internet at http://pubs.acs.org.

JA0104094